A Free Spectroscopic Databank of Infrared Optical Constants for Use in Optics Education and Modeling

Ashley M. Oeck, Russell G. Tonkyn, John S. Loring, Catherine A. Banach,
Ryan M. Francis, Sarah D. Burton, Bruce E. Bernacki, Steven C. Smith, Yin-Fong Su,
James E. Szecsody, Danielle L. Saunders, Tanya L. Myers, Timothy J. Johnson*

Pacific Northwest National Laboratory, 902 Battelle Blvd., Richland, WA, USA 99354

ABSTRACT

The reflectance spectra of solid and liquids can be complicated since they depend not only on absorption, but also on the refraction, reflection, and scattering of light, all of which are wavelength dependent. The physical form and morphological effects associated with solid and liquid samples are thus known to affect their reflectance spectra in a non-linear fashion, particularly in the infrared. Measuring the optical constants $n(\nu)$ and $k(\nu)$ represents an alternative approach, allowing one to model these many effects and thus requiring fewer laboratory measurements. In this paper an overview is presented of the protocols used to measure the n/k optical constants, particularly for liquids. For the liquids, a multiple path length measurements approach is employed, and in this paper we demonstrate the method to determine the complex optical constants $n(\nu)$ and $k(\nu)$ of squalene. The resultant calculated spectra of 1 µm and 100 µm thick layers of squalene on an aluminum substrate as derived from the experimental $n(\nu)$ and $k(\nu)$ values are shown to demonstrate such effects. The public availability of the $n(\nu)/k(\nu)$ data as well as solids hemispherical reflectance data are also discussed.

Keywords: optical constants, refractive index, solids, liquids, database, infrared.

1. INTRODUCTION

In recent years reflectance spectroscopy has come of age as a useful optical technique for identification of solid and liquid materials. The technique has evolved from a somewhat esoteric laboratory technique limited primarily to the optics, semiconductor and fenestration industries to a routine method finding applications from the plane, in the quarry, and on the factory floor.[1-3] Reflectance spectrometers can be found in multiple wavelength ranges including the visible and ultraviolet,[4] as well as more recently in the near-, mid- and far-infrared.[5-7] But interpreting the data for reflectance spectroscopy is far more complicated than for its transmission spectroscopy counterpart. In transmission spectroscopy the signal depends only on the wavelength dependence of the absorption coefficient which is proportional to the complex component of the refractive index $k(\nu)$.[8-10] This is not the case for reflectance spectroscopy as one must take into account not only the absorption of the light, but also its reflection and refraction. These phenomena involve the imaginary component $k(\nu)$ but also the real component $n(\nu)$ of the refractive index.[11-12] The complex refractive index is written as:

$$\tilde{n}(\nu) = n(\nu) + ik(\nu). \tag{1}$$

The optical constants n and k are necessary to understand and model a liquid or solid spectrum with specific morphological conditions. The three effects of absorption, reflectance and refraction all depend on $n(\nu)$ and $k(\nu)$ and also on the angle of incidence and polarization of the light. It is further known that infrared reflectance, emission, and transmission spectra are heavily dependent on the morphology of the sample in question.[13] We have improved upon methods to determine n/k. Originally developed by Bertie,[14-16] the method applies the Kramers-Kronig transform (KKT) to quantitative reflectance $R(\nu)$ and to first determine the phase function $\phi(\nu)$ [as per equation (2)] which can then in turn be employed to obtain the n and k values[7] as determined from equations (3) and (4):

*timothy.johnson@pnnl.gov phone: 509-372-6058

$$\phi(\nu_m) = 2 \, \frac{\nu_m}{\pi} \int_0^\infty \frac{ln\sqrt{R(\nu)}}{\nu^2 - \nu_m} d\nu \tag{2}$$

and

$$n(\nu) = \frac{[1 - R(\nu)]}{\left[1 + R(\nu) - 2\sqrt{R(\nu)}\cos(\phi(\nu))\right]} \tag{3}$$

$$k(\nu) = \frac{-2\sqrt{R(\nu)}\sin(\phi(\nu))}{\left[1 + R(\nu) - 2\sqrt{R(\nu)}\cos(\phi(\nu))\right]} \tag{4}$$

Having determined the $n(\nu)$ and $k(\nu)$ vectors, spectra can be modeled for numerous samples in sundry morphological conditions. In this paper we discuss the methods of using quantitative absorbance data of liquid and solid samples so as to derive the complex infrared optical components. The optical constants of a growing number of liquids and solids are freely available for download from the NIST website[18,24,25] for spectral modeling and other educational purposes.

2. EXPERIMENTAL

2.1 Liquids Measurements

The experimental methods use to derive the liquids $n(\nu)$ and $k(\nu)$ optical constants data were largely derived by Bertie and colleagues[7,14-16] and improvements to these methods have been described by Myers et al.[18-19] While the basic experimental procedure involves making a series of simple liquids transmission measurements, attention to detail is required at every step in order to obtain quantitative values for k (and in turn for n).

The key to quantitative results lies within the multiple path length method of data collection for liquid samples. This approach allows for more accurate analysis where the signal may vary up to four orders of magnitude between the weak and strong absorption bands. In addition, liquid absorbance measurements are now recorded in both the mid-infrared (MIR) and near-infrared (NIR) regions, with data extended[19] out to 10,000 cm^{-1}. Shorter path length cells are used for MIR measurements where strong absorbance features have become saturated (ABS$_{10} \geq 2$). Such features are usually associated with fundamental modes of vibration and typically lie between 4,000 and 400 cm^{-1}. Longer path lengths are used for the weaker absorption bands above 4,000 cm^{-1}. Inclusion of NIR measurements allows for detection of weak absorption features above ca. 5,000 cm^{-1} and greatly improves signal-to-noise (S/N).

Two different FTIR spectrometers are used in order to optimize each instrument for their respective spectral region of interest and to increase the efficiency of sample collection time. NIR measurements (10,000-3,000 cm^{-1}) are recorded on a Bruker Vertex 70 using a quartz tungsten bulb, an extended-range broadband potassium bromide (KBr) beamsplitter and a deuterated triglycine sulfate (DTGS) detector. A Bruker Tensor 27 with a silicon carbide glow bar source, broadband potassium bromide (KBr) beamsplitter and a DTGS detector is used to collect MIR data ranging from 7,800 to 400 cm^{-1}. An empty sample chamber purged with ultra-high purity nitrogen gas is used as a background (I_0) spectrum. Absorbance spectra are then generated by using the equation $A = -\log(I/I_0)$ where I is the sample spectrum. Typically three sets of 128 scans are collected at 2.0 cm^{-1} resolution for each sample.

Prior to sample measurements, daily tests are performed to calibrate both the x and y-axes (frequency and transmission values, respectively). The x-axis is calibrated using gas-phase CO_2 and H_2O reference data from the Pacific Northwest National Laboratory (PNNL) IR database[20] in comparison to measured absorbance spectra of the sample compartment open to air. The y-axis is calibrated using a MRC Infrared Linearity Standard (MRC-910-NG11 S/N 0108, Middleton Spectral Vision, Middleton, WI) with known transmission values compared at various wavelengths. The sample used as an example in the manuscript is squalene from Alfa Aesar (98% purity).

To provide quantitative values for both *n* and *k*, multiple path lengths are used to account for both strong and weak absorption bands. Weaker absorption features above ~4,000 cm^{-1} are also detected by employing the MIR-NIR dual measurement protocol. As shown in Figure 1, commercial cells utilized for liquid absorbance measurements are typically made of potassium bromide (KBr) with path lengths ranging from 15 µm to 3,000 µm, but potassium chloride or zinc selenide (for aqueous species) may also be used. To provide accurate results for stronger absorbance bands, shorter path cells are formed by placing the 15 µm cells in a hydraulic press to achieve path lengths down to as short as 1.5 µm. For the MIR at least seven different path lengths are used between 1 and 500 µm. In the NIR 100, 200, 500, 1,000 and 3,000 µm cells are used. For consistency purposes and to aid in the data merging process, the same 100, 200 and 500 µm cells with the same fill are used for both the MIR and the NIR instruments/measurements.
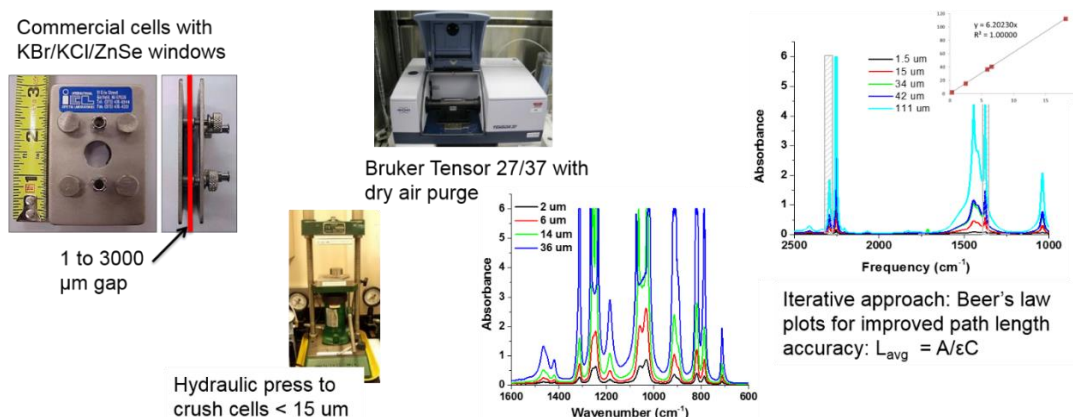

Figure 1: Instrumentation used to provide quantitative data. A Bruker Tensor 27 or 37 is used to measure absorbance spectra of liquids injected into commercial cells ranging from 15 to 3,000 µm. For saturated bands, cells must be crushed with a hydraulic press to achieve path lengths < 15 µm. Beer's law is utilized to estimate cell path lengths based on certain bands.

Path length values are initially estimated by measuring the fringe spacing in an empty cell, but further analysis is required to account for changes that may result from cells relaxing after being filled. An iterative approach based on the Beer-Lambert law of absorption is used to determine the ratio of path lengths for various cells from multiple absorbance plots in order to get the best estimate of path lengths.

In addition to the multiple path length approach, multiple burdens (i.e. replicate sample fills and measurements) are used for each path length to provide accurate measurements over a range of varying band strengths. Shorter path lengths are key for the accuracy of strong absorption bands and achieving linearity, while longer path length cells and the extension of collection methods to the near-infrared provide further information about weaker absorbance features. The *k* vectors are calculated for each absorbance file using[21] Bertie's program "RNJ46A" and appropriate regions from each are later merged to provide a composite *k* vector.

In addition to absorbance measurements, the refractive index of liquid samples is measured using an ATAGO refractometer at seven fixed wavelengths in both the visible and near-IR region. The scalar *n* values are measured at 480, 486, 546, 589, 644, 656 and 1,550 nm and a modified-Sellmeier equation[22] is used to interpolate *n* at the highest frequency value:

$$n(\lambda) = A + \left(\frac{B}{\lambda^2 - C}\right)^{1/2} \tag{5}$$

The final *n* vector is calculated using the composite *k* vector and the refractive index at the highest frequency value using the Kramers-Kronig relation[21] per Bertie's "LZZKTB" program.

2.2 Solids and Bulk Liquid Measurements

The methods used to acquire the hemispherical and diffuse reflectance spectra in the mid-infrared using an integrating sphere have been previously described.[3,4,23,24] An integrating sphere coupled to a spectrometer can be used to measure the reflectance spectra of solids, bulk liquids and samples deposited on various substrates. Briefly, a 75 mm matte gold-coated Bruker A562 integrating sphere accessory with a two-port design is placed in the sample compartment of a Bruker Tensor 37 FTIR, or bolted to a Bruker Optics IR Cube FTIR spectrometer. The spectrometer provides a modulated infrared beam to the sphere which is reflected by a flip mirror located inside the integrating sphere. The flip mirror is used to reflect light directly to the sample at the bottom port or to a point of reference (either top port or side wall) within the sphere. With the mirror pointing down towards the sample port, a 15° angle is formed between the incident light beam and the normal to the sample surface (Figure 2).

Per the two-port design, two sets of spectra can be recorded for each sample: the diffuse-only reflectance spectra (where the specular component is removed) and total (or hemispherical) reflectance spectra. For hemispherical reflectance as shown in Figure 2A, the top gold dome is left in place so that the light comes in from the right, reflects off a mirror and down to the sample where all the reflected light is collected. The specular ray is indicated in the red arrows, while the diffuse components are shown in green. For diffuse-only measurements depicted in Figure 2B, the top gold dome is removed to allow the specular component to escape.
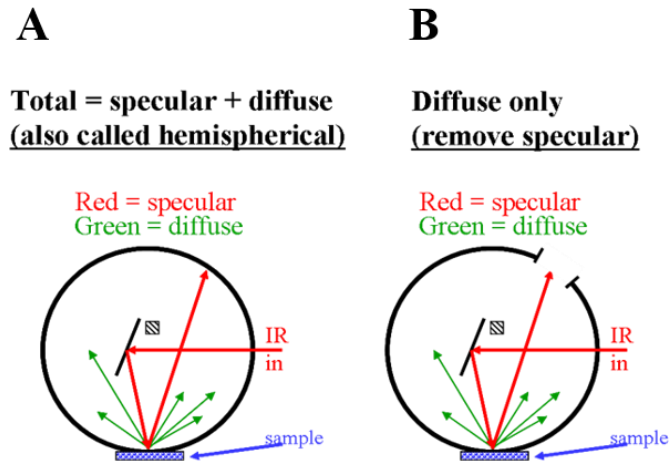

Figure 2: Sketch of the integrating sphere used to take hemispherical (A) and diffuse-only (B) measurements where the gold dome top is removed to allow the specular portion to escape. The black hatched square represents the detector on the axis going into the paper.

Hemispherical and diffuse-only reflectance spectra were collected using a double-sided, forward-backward acquisition at 4.0 cm⁻¹ resolution between 7,500 and 500 cm⁻¹, using a Mertz phase correction and a Blackman-Harris 3-term apodization. The instrument is purged with ultra-high purity N_2 to reduce excess H_2O and CO_2 interferences. A set of standards is measured daily prior to collecting sample spectra to ensure the instrument and its reflectance accessory are performing consistently and optimally.

3. RESULTS AND DISCUSSION

3.1 Typical case for liquids: Squalene

Squalene is presented as an example in this manuscript where various peak strengths are present throughout the entire spectral range (10,000 to 400 cm⁻¹, 1.0 to 25.0 µm) and multiple path lengths are necessary to determine accurate k (and therefore n) values. Shorter path lengths are important for maintaining a linear response for the strong bands. The longer path lengths are necessary, however, to detect weaker band strengths above 6,000 cm⁻¹, in particular to achieve good S/N in this domain. Seven cells with varying path lengths (6.03, 9.23, 19.3, 42.9, 121, 262 and 503 µm) were used for

absorbance measurements of squalene for the MIR to account for varying band strengths as demonstrated in Figure 3 (left). Five path length cells were used for the NIR absorbance measurements: 122, 260, 508, 1,024 and 3,055 µm (right). The 122, 260 and 508 µm cells used in the NIR measurements were the same cells from the MIR measurements with the same fill. Since MIR and NIR path lengths are calculated independently from each other and based on their absorbance spectra, marginal differences in values from the same cell may be a result of the cell relaxing or minor differences in the Beer-Law plots, the differences less than 2% in almost all cases. Since two spectrometers are used, a slightly different portion of the liquid cell may be interrogated by the beam. As shown from Figure 3, multiple path lengths are necessary to account for regions of the spectra where peaks become saturated or conversely, where signal is very weak, but a feature is indeed present.
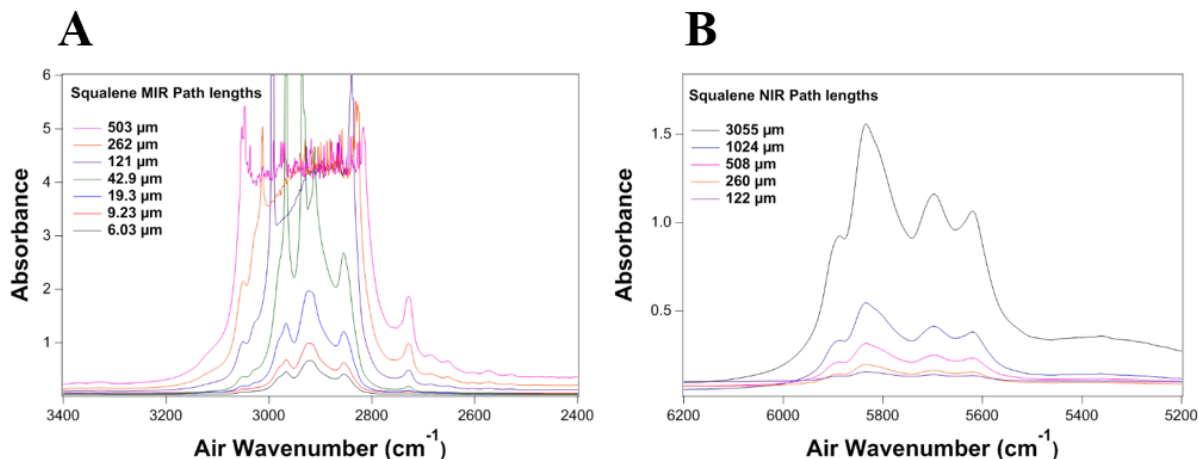

Figure 3: Example of multiple path lengths used for squalene for the MIR (A) and NIR (B) absorbance measurements. MIR data in this figure are presented from 3,400 cm^{-1} to 2,400 cm^{-1} while NIR data are presented between 6,200 and 5,200 cm^{-1}. Seven path lengths were used for the MIR (6.03, 9.23, 19.3, 42.9, 121, 262 and 503 µm) and 5 for the NIR (122, 260, 508, 1,024 and 3,055 µm). The same cells with the same fill of squalene were used for the 121-503 µm path lengths for both instruments.

Figures 3A and 3B demonstrate the importance of using multiple path lengths: For the MIR peak near 3,000 cm^{-1} the long path cells (121, 262 and 503 µm) are all off scale with measurements of ABS >3; these data are not used in the fit at these wavelengths. However, the same cells represent good data (linear in response) in the NIR near 5,700 cm^{-1}, along with two additional long path cells of 1,024 and 3,055 µm. Using such data, individual *k* vectors were created for each path length cell for both MIR and NIR data and then merged to create a composite *k* vector for each region. For the NIR three vectors were created and merged by hand to create a final *k*-vector for the NIR region between 10,000 and 3,601 cm^{-1}. For the MIR, five composite spectra were created and merged to produce the final MIR *k*-vector between 7,800 and 400 cm^{-1}. A more detailed list of the individual *k*-vectors and their regions is provided in Table 1.

Table 1. List of cells used to create individual MIR and NIR *k*-vectors and their corresponding spectral regions.

MIR *k*-vectors		NIR *k*-vectors	
Region (cm^{-1})	Cell Paths (µm)	Region (cm^{-1})	Cell Paths (µm)
7,800 – 4,777 2,711 – 1,616 688 – 400	121, 262 and 509	10,000 – 7,543	1024 and 3055
4,777 – 3,639	42.9, 121, 262 and 509	7,543 – 4,776	508, 1024 and 3055
3,639 – 2,711	6.03, 9.23 and 19.3	4,776 – 3,601	122, 260, 508 and 1024
1,616 – 1,293	19.3 and 42.9		
1,293 – 688	6.03, 19.3 42.9 and 121		

The refractive index for squalene was calculated at 27 °C at seven wavelengths using an Abbe Refractometer to determine (via interpolation) the n value at the highest recorded IR frequency for both the MIR (7,800 cm^{-1}) and NIR (10,000 cm^{-1}). Using a modified-Sellmeier fit, the refractive index was determined via interpolation to be 1.4771 at 10,000 cm^{-1} and 1.4730 at 7,800 cm^{-1} as seen in Figure 4.

Point	'Wavelength	RI
0	0.4800	1.5029
1	0.4860	1.502
2	0.5460	1.496
3	0.5890	1.4928
4	0.6440	1.49
5	0.6560	1.4893
6	1.5500	1.4708

At 10000 cm^{-1} n =1.4771
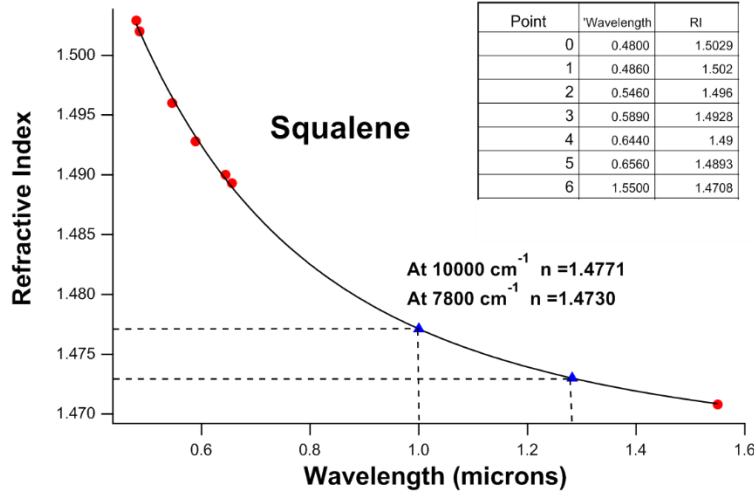At 7800 cm^{-1} n =1.4730

Figure 4: Plot of measured refractive index values collected with Abbe refractometer (red circles) along with the modified Sellmeier fit (black trace) for squalene at 27 °C. The dashed lines and blue triangles represent where the refractive index at 10,000 cm^{-1} and 7,800 cm^{-1} was determined from the fit via interpolation.

A composite k-spectrum between 10,000 and 400 cm^{-1} was created from the composite MIR and NIR k vectors. The NIR data were used exclusively above 5,577 cm^{-1} and the MIR data were used exclusively below 4,853 cm^{-1}. The overlap region between MIR and NIR data was between 5,577 and 4,853 cm^{-1}. The KKT per Bertie's[21] program "LZZKTB" was used to create a final n vector from the resulting composite k vector and the refractive index at the highest frequency for the spectral region (10,000 cm^{-1}). The final composite $n(\nu)$ and $k(\nu)$ spectra are shown below in Figure 5 across the entire spectral domain. By using multiple path lengths and a two-instrument system to accommodate MIR and NIR measurements, both strong and weak absorption features were detected for squalene and more accurate $n(\nu)$ and $k(\nu)$ values were derived across a large spectral range.
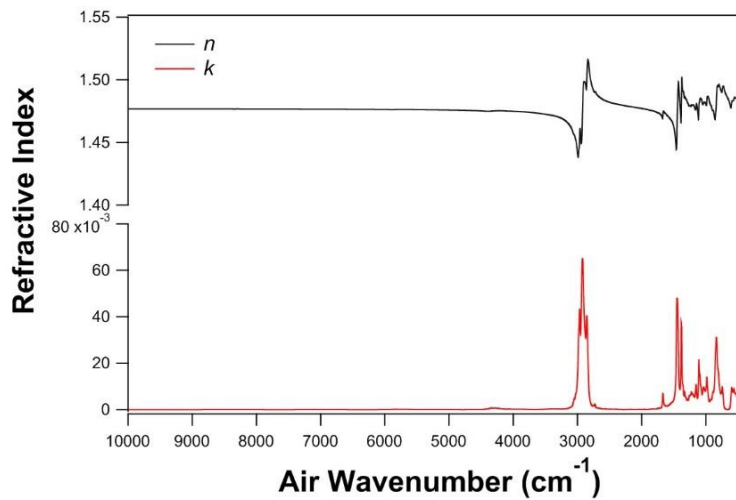

Figure 5: The final n (black trace) and k (red trace) spectra of squalene over 10,000-400cm^{-1}.

3.2 Modeling spectra based on $n(\nu)$ and $k(\nu)$

Optical constants can be useful in modeling samples that may be encountered in an environment other than bulk liquids. This is important because other than water, the bulk form is rarely encountered for liquids, but rather as thin/thick layers on substrate, droplets, aerosols, etc. Reflectance measurements of liquids are thus more complicated as absorbance, reflectance and refraction of the incident light must all be taken into account. So-called "transflectance" features are prominent in thin layer systems as the incidence light can pass through the sample multiple times. As an example, we have used the $n(\nu)$ and $k(\nu)$ values derived above to calculate model spectra of 1 µm and 100 µm layers of squalene on aluminum as seen in Figure 6. To produce these spectra, a commercial thin film modeling and design package (Essential Macleod) was used with an incidence angle of 60°. As shown, spectra can vary drastically based on morphological conditions such as particle size, substrate material, and layer thickness.
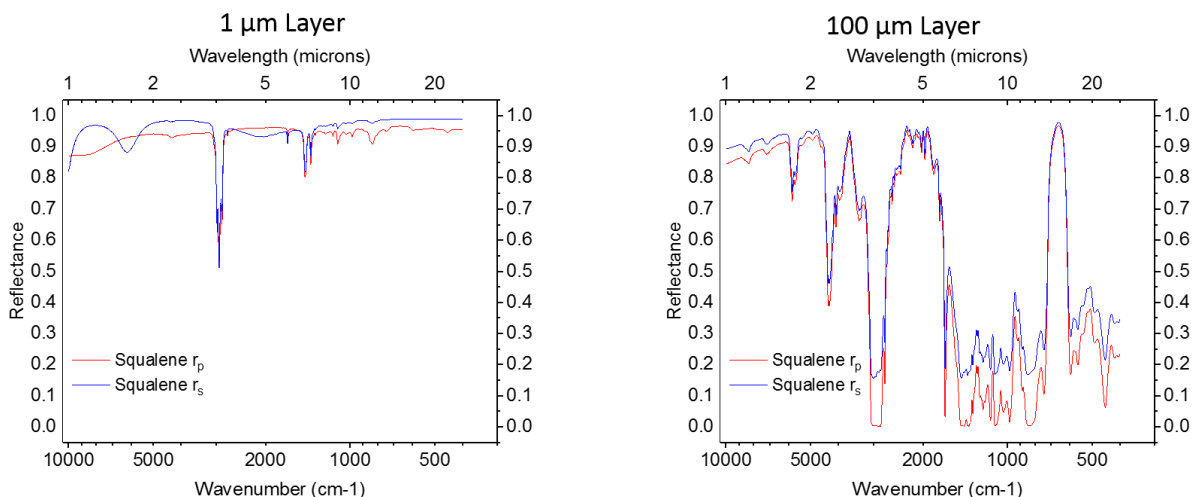

Figure 6: Modeled reflectance spectra of squalene at two different thicknesses on aluminum. Two different polarizations are shown for the reflected light.

3.3 Publicly available data

Currently the optical constants for 57 liquid species spanning a diverse set of organic, inorganic and organophosphorous compounds are available on the NIST website at https://webbook.nist.gov/chemistry/silmarils-liquids-n-k/.[18,24] For this set of compounds, n and k values are available from 7,800 to 400 cm^{-1} at 2 cm^{-1} resolution. An additional 70 liquids have been measured using the MIR-NIR dual method to extend data out to 10,000 cm^{-1}. These compounds have been detailed in a previous publication and will be available for download at a later date.[19]

In addition to the liquids n/k data, quantitative values for hemispherical and diffuse reflectance is available for download for 130 solid samples on the NIST website (https://webbook.nist.gov/chemistry/silmarils-solids-hrf-drf/).[13,25] The optical constants of solids using quantitative absorption measurements in KBr pellets have also been recorded as outlined by Myers et al.[26] Specifically, the n/k values for 70 solids of both inorganic and organic species have been calculated using this method. Due to the limited availability of optical constants for solid compounds, more experiments are required to confirm the validity of the KBr pellet method.

4. SUMMARY

The determination of the optical constants n and k is useful for modeling the reflectance spectra of samples encountered outside of laboratory norms. As reflectance spectroscopy becomes a more applied method, we have augmented those efforts by creating a free spectroscopic database of infrared optical constants for both solid and liquid materials. Currently, a library of optical constants for roughly 60 liquid species is freely available for download, with more species to be added.[24]

We have summarized the methods used to collect accurate quantitative optical constants for liquid samples and have demonstrated how morphology can affect reflectance spectra with squalene as an example. Techniques to provide optical constants for solid samples are also being developed, with the use of absorption spectroscopy for analytes in KBr pellets.

ACKNOWLEDGEMENTS

REFERENCES

[1] Griffiths, P. R. and de Haseth, J. A., "Fourier Transform Infrared Spectroscopy," John Wiley and Sons Inc.: New York, 1986.

[2] Hanssen, L., "Integrating-sphere system and method for absolute measurement of transmittance, reflectance, and absorptance of specular samples," Applied Optics 40(19), 3196-3204 (2001).

[3] Blake, T. A. et al., "Methods for quantitative infrared directional-hemispherical and diffuse reflectance measurements using an FTIR and a commercial integrating sphere," Applied Optics 57(3), 432-446 (2018).

[4] Johnson, T. J., Bernacki, B. E., Redding, R. L. et al., "Intensity-Value Corrections for Integrating Sphere Measurements of Solid Samples Measured Behind Glass," Applied Spectroscopy, 68(11), 1224-1234 (2014).

[5] Russell, E. E. and Bell, E. E., "Measurement of the Optical Constants of Crystal Quartz in the Far Infrared with the Asymmetric Fourier-Transform Method," J. Opt. Soc. Am. 1967, 57 (3), 341-348.

[6] Sani, E. and Dell'Oro A., "Corrigendum to "Optical constants of ethylene glycol over an extremely wide spectral range," Optical Materials 48, 281 (2015).

[7] Lund-Myhre, C. E., Grothe, H., Gola, A. A. and Nielsen, C. J., "Optical Constants of HNO_3/H_2O and $H_2SO_4/HNO_3/H_2O$ at Low Temperatures in the Infrared Region," J. Phys. Chem. A 109, 7166-7171 (2005).

[8] Lindenmaier, R., Scharko, N. K., Tonkyn, R. G., Nguyen, K. T., Williams, S. D. and Johnson, T. J., "Improved assignments of vibrational fundamental modes of ortho-, meta-, and para-xylene using gas- and liquid-phase infrared and Raman spectra combined with ab initio calculations: quantitative gas-phase infrared spectra for detection," J. Mol. Struct. 1149, 332-351 (2017).

[9] Profeta, L. T. M., Sams, R. L., Johnson, T. J. and Williams, S. D., "Quantitative infrared intensity studies of vapor-phase glyoxal, methylglyoxal, and 2,3-butanedione (diacetyl) with vibrational assignments," J. Phys. Chem. A 115, 9886-9900 (2011).

[10] Johnson, T. J., Aker, P. M., Scharko, N. K. and Williams, S. D., Quantitative infrared and near-infrared gas-phase spectra for pyridine: Absolute intensities and vibrational assignments," Journal of Quantitative Spectroscopy & Radiative Transfer 206, 355–366 (2018).

[11] DeVetter, B. M., Scharko, N. K., Cannon, B. D., Myers, T. L. and Johnson, T. J., "Single-angle reflectance spectroscopy to determine the optical constants n and k: considerations in the far-infrared domain," Applied Optics 2018, 57 (22), 6587-6597.

[12] DeVetter, B. M., Myers, T. L., Cannon, B. D., Scharko, N. K., Kelly-Gorham, M. K., Corbey, J. F. and Schemer-Kohrn, A. L., "Optical and chemical characterization of uranium dioxide (UO_2) and uraninite mineral: Calculation of the fundamental optical constants," Journal of Physical Chemistry A. 122(35), 7062-7070 (2018).

[13] Myers, T. L., Brauer, C. S., Su, Y-F. et al., "Quantitative reflectance spectra of solid powders as a function of particle size," Applied Optics 54(15), 4863-4875 (2015).

[14] Bertie, J. E., Zhang, S. L. and Keefe, C. D., "Measurement and use of absolute absorption intensities of neat liquids," Vib. Spectrosc. 8, 215-229 (1995).

[15] Bertie, J. E., Keefe, C. D. and Hones, R. N., "Infrared intensities of liquids VIII. Accurate baseline correction of transmission spectra of liquids for computation of absolute intensities, and the 1036 cm-1 band of benzene as a potential intensity standard," Can. J. Chem. 69, 1609-1618 (1991).

[16] Bertie, J. E., Zhang, S. L. and Keefe C. D., "Infrared intensities of liquids XVI. Accurate determination of molecular band intensities from infrared refractive index and dielectric constant spectra," J. Mol. Struct. 324, 157-176 (1994).

[17] Lund Myhre, C. E., Christensen, D. H., Nicolaisen, F. M. and Nielsen, C. J., "Spectroscopic study of aqueous H_2SO_4 at different temperatures and compositions: variations in dissociation and optical properties," J. Phys. Chem. A. 107, 1979-1991 (2003).

[18] Myers, T. L., Tonkyn, R. G., Danby, T. O., Taubman, M. S., Bernacki, B. E., Birnbaum, J. C., Sharpe, S. W. and Johnson, T. J., "Accurate Measurement of the Optical Constants n and k for a Series of 57 Inorganic and Organic Liquids for Optical Modeling and Detection," Appl. Spec. (2017); https://doi.org/10.1177/0003702817742848

[19] Myers, T. L., Tonkyn, R. G., Loring, J. S., Oeck, A. M., Banach, C. A., Francis, R. M., Su, Y-F. and Johnson, T. J., "Accurate optical constants for liquids in the near-infrared: Improved methods for obtaining the n and k constants from 1 to 4 µm," Proc. SPIE 11010, Chemical, Biological, Radiological, Nuclear and Explosives (CBRNE) Sensing XX, 110100O (2019).

[20] Sharpe, S. W., Johnson, T. J., Sams, R. L., Chu, P. M., Rhoderick, G. C. and Johnson, P. A., "Gas-phase databases for quantitative infrared spectroscopy," Appl. Spectrosc. 2004, 58 (12), 1452-1461.

[21] Bertie, J. E., "John Bertie's Download Site," May 14, 1997, <https://sites.ualberta.ca/~jbertie/JBDownload.HTM> (20 May 2019).

[22] Tatian, B., "Fitting refractive-index data with the Sellmeier dispersion formula," Appl. Opt. 23(24), 4477-4485 (1984).

[23] Blake, T. A., Johnson, T. J., Tonkyn, R. G., Forland, B. M., Myers, T. L., Brauer, C. S. and Su, Y-F., "Quantitative Total and Diffuse Reflectance Laboratory Measurements for Remote, Standoff, and Point Sensing," Chemical, Biological, Radiological, Nuclear, and Explosives (CBRNE) Sensing XV. 2014. 9073

[24] Myers, T. L., Tonkyn, R. G, Oeck, A. M., Danby, T. O., Loring, J. S., Taubman, M. S., Sharpe, S. W., Birnbaum, J.C. and Johnson, T. J., "IARPA / PNNL Liquid Phase IR Spectra," NIST Chemistry Webbook, October 2018, https://webbook.nist.gov/chemistry/silmarils-liquids-n-k/ (20 May 2019).

[25] Johnson, T. J., Myers, T. L., Su, Y-F., Tonkyn, R. G., Kelly-Gorham, M.-R. K. and Danby, T. O., "IARPA / PNNL Solid Phase IR Spectra," NIST Chemistry Webbook, October 2018, https://webbook.nist.gov/chemistry/silmarils-solids-hrf-drf/ (20 May 2019).

[26] Myers, T. L., Francis, R. M., Banach, C. A., Burton, S. D., Oeck, A. M., Johnson, T. J., Furstenberg, R. and Kendziora, C. A., "Obtaining the complex optical constants n and k via quantitative absorption measurements in KBr pellets," Proc. SPIE 11010, Chemical, Biological, Radiological, Nuclear and Explosives (CBRNE) Sensing XX, 110100M (2019).